Test particle transport in perturbed magnetic fields in tokamaks

M. de Rover, A. M. R. Schilham, A. Montvai, and N. J. Lopes Cardozo
FOM-Instituut voor Plasmafysica ''Rijnhuizen,'' Association Euratom-FOM, Trilateral Euregio Cluster, P.O. Box 1207, 3430 BE Nieuwegein, The Netherlands

(Received 10 November 1998; accepted 8 March 1999)

Numerical calculations of magnetic field line trajectories in a tokamak are used to investigate the common hypotheses that (i) field lines in a chaotic field make a Gaussian random walk and (ii) that the poloidal component of the magnetic field is uniform in regions with a chaotic magnetic field. Both hypotheses are found invalid in typical tokamak conditions. A test particle transport model in the so-called ''collisionless diffusion'' limit is presented, based on the field line excursions in numerical simulations. Decorrelation mechanisms that effectively enhance the transport in a stochastic field are investigated. © *1999 American Institute of Physics.* [S1070-664X(99)02406-4]

I. INTRODUCTION

Tokamaks[1] confine thermonuclear plasmas in a torus by a helical magnetic field. To a good approximation, the field lines lie on nested toroidal surfaces, so-called flux surfaces. Transport perpendicular to those surfaces is 10–12 orders of magnitude smaller than the transport along the field lines, so that the flux surfaces are effectively isothermal and isobaric surfaces. Experimental observations show that the cross-field ion heat conduction is a few times larger than predicted by neoclassical theory, which assumes that radial transport only arises when particles move from surface to surface by collisions. For the electron heat transport the anomaly is even one to two orders of magnitude.

Generally, electrostatic turbulence is invoked to explain the anomaly.[2] Recently, conditions have been achieved in the DIII-D tokamak,[3] in which the ion heat conduction dropped to the neoclassical value, while the electrostatic turbulence level became vanishingly small. However, the electron heat conduction did stay strongly anomalous.

A possible cause for the anomalous electron heat conduction is magnetic turbulence (see, e.g., Ref. 4). A rough estimate shows that the radial excursions of field lines due to a perturbing field $b_\epsilon = \tilde{B}/B = 10^{-4}$, could significantly enhance the electron heat transport. Measurements of the magnetic fluctuations in Tore Supra[5] did yield $b_\epsilon \sim 10^{-5} - 10^{-4}$, while ultrahigh resolution measurements of the electron temperature profile in the Rijnhuizen Tokamak Project (RTP)[6] show coherent structures compatible with perturbing fields of $b_\epsilon \lesssim 10^{-3}$. Thus, there is an incentive for investigations of thermal transport in a tokamak plasma with a slightly perturbed magnetic field.

Concerning the magnetic field, it should be noted that the field line equations for a time independent magnetic field in a tokamak are analogous to Hamilton's equations:

$$\frac{d\psi_t}{d\phi} = -\frac{\partial \psi_p}{\partial \bar{\theta}}, \quad \frac{d\bar{\theta}}{d\phi} = \frac{\partial \psi_p}{\partial \psi_t}. \tag{1}$$

In this, we have to make use of a coordinate system $(r, \phi, \bar{\theta})$, expressing the minor radius, the toroidal angle, and a poloidal angle, which is like the conventional poloidal angle θ. Then $2\pi\psi_t$ and $2\pi\psi_p$ can be identified as the toroidal and poloidal magnetic flux in the magnetic field picture, or we can regard Eq. (1) as Hamilton's equations, with $\psi_p(\psi_t, \phi, \bar{\theta})$ the Hamiltonian and ϕ the time coordinate.

From this analogy, it can be concluded that it is a generic, mathematical property that surfaces on which field lines close back on themselves after a finite number of toroidal turns are topologically unstable.[7] So-called ''magnetic islands'' will form as is apparent in the universal representation of slightly perturbed Hamiltonian systems near closed trajectories.[8] Where islands overlap, regions with chaotic field line trajectories will arise. For sufficiently small b_ϵ, these regions are limited, so that good surfaces remain [Kolmogorov Arnold Moser (KAM) theorem[8]]. Hence, the generic topology of the field in a tokamak consists of magnetic islands, regions with good surfaces, and chaotic regions.

There is an extensive literature on (transport in) chaotic magnetic fields (see, e.g., Refs. 9–13). These papers use the assumption that in a chaotic region, neighboring field lines diverge exponentially. The exponential divergence shows up in the time needed for a particle to decorrelate from a field line. The process is often visualized by following the evolution of the cross section of a bunch of correlated field lines on their way around the torus. The cross section, which is taken circular (with a radius equal to the perpendicular correlation length of field lines) at the start, is assumed to develop into a complex structure of thin long arms spreading in various directions.

A particle moving along the bunch of field lines gradually moves away from its initial field line (e.g., due to collisions), while at the same time the bunch deforms into a shape with ever thinner arms. A particle is said to be completely decorrelated from the initial field line when its distance from this field line equals the width of the arms at that moment. This defines the decorrelation time τ, and the parallel decorrelation distance $z(\tau)$.

The radial distance traveled $\rho(z(\tau))$, is then obtained from a suitable model of the field line excursions. Usually, the Rechester and Rosenbluth[9] formula for the scaling of the diffusivity χ with the test particle velocity $v_\parallel$ along the field

line, is used to compute test particle transport in a stationary chaotic field:

$$\chi = D_M v_{\parallel}. \tag{2}$$

The ''magnetic diffusion coefficient,'' D_M, can be approximated by the quasilinear[7] estimate $D_M \sim L_{c\parallel} b_\epsilon^2$, when $b_\epsilon L_{c\parallel} \ll L_{c\perp}$, with $L_{c\parallel}$ and $L_{c\perp}$ denoting the longitudinal and transversal correlation lengths of the perturbing magnetic field. Formula (2) pertains to the so-called ''collisionless diffusion'' regime, which is applicable when $t_d < \tau_c$. Here τ_c is the collision time and $v_{\parallel} t_d$ is the length along a field line after which a radial displacement by one gyroradius (ρ_e) is sufficient to move the test particle to an uncorrelated field line. The validity of Eq. (2) and the quasilinear estimate of D_M has been the subject of much discussion in the literature (examples are Refs. 4, 13, and 14), regarding the decorrelation mechanisms involved in the resulting time and spatial scales lengths.

Summarizing, there are three essential ingredients for calculating test particle transport: (i) the model for the decrease of the arm widths; (ii) the model for the radial excursions of field lines; (iii) the assumption of a stationary chaotic field. In this paper, we will investigate the validity of the first two assumptions. To this end, we will use arguments arising from a sophisticated numerical code as well as analytical ones.

II. NUMERICAL IMPLEMENTATION

To generate large numbers of different magnetic field realizations we developed a set of computer programs based on so-called mapping functions.[15,16] Dividing the torus in a number of cross sections, covered with rectangular grids, we compute the magnetic field on each grid point, as the sum of an ideal field $\mathbf{B}_0$ and a (small) perturbing part $\mathbf{B}_\epsilon$ that causes the chaotic behavior of the field lines (technical details of the numerical procedures can be found in the Appendix). For the unperturbed tokamak field of our numerical model we used

$$\mathbf{B}_0(x,\theta) = \frac{B_0}{1 + x\cos\theta}\left(\mathbf{e}_\phi - \frac{x}{q(x)}\mathbf{e}_\theta\right) \tag{3}$$

in the right-handed toroidal coordinate system ($x = r/R_0, \phi, \theta$), i.e., the ratio of the distance to the magnetic axis over the major radius, the toroidal angle, and the poloidal angle, with orthonormal basis vectors $\mathbf{e}_x$, $\mathbf{e}_\phi$, and $\mathbf{e}_\theta$. This tokamak field (3) is known in the literature as the standard model,[17] giving the correct magnetic field in the large aspect ratio approximation $a/R_0 \ll 1$ with a the minor radius of the tokamak, and satisfying $\nabla \cdot \mathbf{B}_0 = 0$.

The safety factor $q(x)$ is a dimensionless function, expressing the pitch angle of the magnetic field. For a cylindrical plasma carrying a plasma current $I_{\rm pl}(x) = 2\pi R_0^2 \int_0^x j(x)\, x\, dx$, with $j(x)$ the current density, q is written

$$q(x) = q_{\rm cyl} = \frac{2\pi x^2 R_0 B_0}{\mu_0 I_{\rm pl}(x)}. \tag{4}$$

For our model, $q(x)$ takes the (realistic) parabolic form[18]

$$q(x) = q_0 + (q_a - q_0)\frac{x^2 R_0^2}{a^2}, \tag{5}$$

with $q_0 = 0.8$ the value at the magnetic axis and $q_a = 4.5$ at the plasma edge. For the torus, parameters of RTP are used: $R_0 = 0.72$ m, $B_0 = 2.2$ T, minor radius 0.16 m.

For the perturbing field, two limiting cases have been used in separate simulations: (i) very localized perturbations to the current density profile induced by small closed current filaments[16] and (ii) the conventional model of less localized, ''global,'' perturbations to the magnetic flux in the form of a sum of Fourier components resonant at surfaces with rational q.

Current filaments are modeled as closed current carrying wires running parallel to magnetic field lines on rational surfaces of the unperturbed field. A set of filaments is chosen such that their total current is zero. The perturbing field is the sum of the fields of all filaments. Using a current (rather than flux) distribution to compute $\mathbf{B}_\epsilon$ has the advantage that unphysical situations [e.g., often the flux perturbations taken in the literature (see, e.g., Ref. 19) have no radial dependence, which corresponds to a diverging current density on the magnetic axis] are avoided. Moreover, this setup provides a way to numerically handle systems that in a flux representation would require extremely long Fourier series.

Knowing the magnetic field on each grid point, the field line equations are solved between cross sections to construct mapping functions. With simple but effective interpolation schemes, these mapping functions give the position of a field line at a particular cross section given its position at the previous cross section. As all the information of the field is stored in the mapping functions this method allows one to trace any number of field lines simultaneously. The CPU-time consumed in the mapping construction process is paid off by the interpolation process, making this method faster than conventional schemes that integrate the field line equations for each field line individually.

Both the filaments and the Fourier series perturbations produced the generic layered topology, with islands and stochastic regions [Figs. 6(a) and 6(d) for the system with filaments]. However, the Fourier perturbations needed a larger b_ϵ by a factor 10, than the filaments to produce chaotic zones of similar width. This results from the fact that global modes contribute to b_ϵ also where they are not resonant, i.e., where they do not cause field stochastization, whereas the effect of the filaments is concentrated near their resonances.

For the perturbations, we used Fourier mode numbers up to $m = 15$ or up to 21 filaments.

As an example of a chaotic magnetic field generated with the code, Fig. 1 gives the Poincaré plot for a field perturbed with a set of 19 filaments, each carrying on average 0.05% of the total plasma current. The perturbing field had a strength $b_\epsilon = B_\epsilon / B_0 \approx 10^{-3}$. This is an upper limit for what is expected in a tokamak (10^{-4} is measured by Zou *et al.* in Ref. 5), and is suitable to make our points clear.

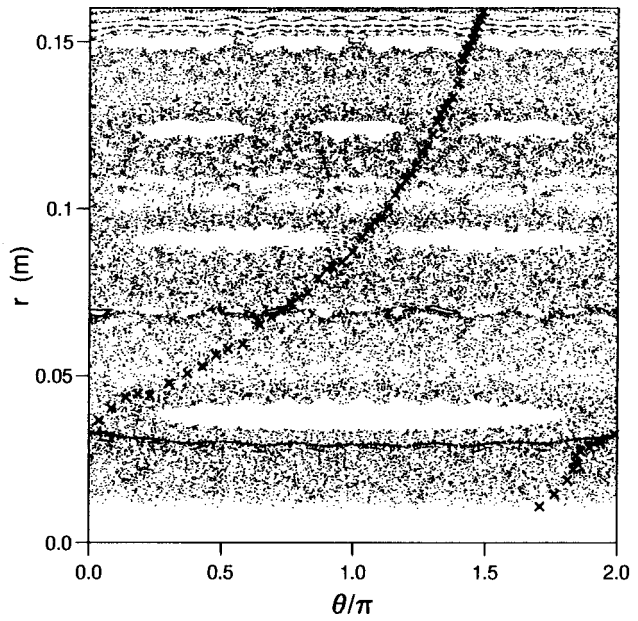

FIG. 1. Poincaré plot for a magnetic field perturbed by a large number of small current filaments producing a perturbation level $b_\epsilon \approx 10^{-3}$. For the unperturbed magnetic field, parameters of the Rijnhuizen Tokamak Project are used: minor radius $a=0.16$ m, major radius $R=0.72$ m; toroidal magnetic field $B=2.2$ T; $q(r)=q(0)+(q(a)-q(0))r^2/a^2$, $q(a)=4.35$, $q(0)=0.8$. The 60 orbits plotted here for 600 transits each are denoted by crosses after one transit.

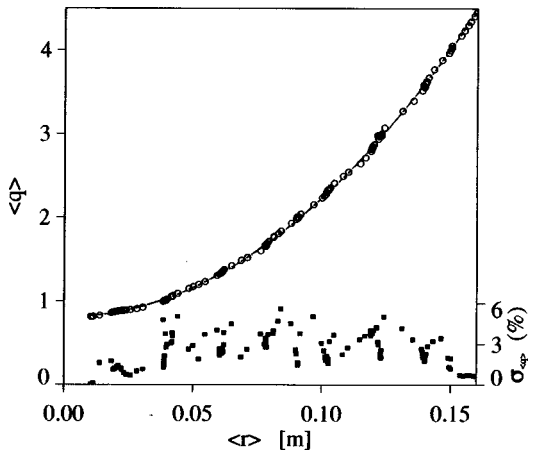

FIG. 2. $\langle q\rangle$ as a function of the average radial coordinate $\langle r\rangle$ of a field line. Gray line: unperturbed magnetic field; circles: results for 150 initial radial positions, averaged over 100 initial angles θ each and 100 toroidal turns, for $b_\epsilon \approx 10^{-3}$ (see Fig. 1); boxes: standard deviation $\sigma_{\langle q\rangle}$ of $\langle q\rangle$.

III. IMPORTANCE OF SHEAR IN CHAOTIC MAGNETIC FIELD

Theories of transport in chaotic magnetic fields commonly neglect the effect of magnetic shear (i.e., a nonuniform q) in the chaotic regions (see Refs. 9, 12, and 13, and for very weak shear see Ref. 10). In tokamaks, magnetic shear results from the nonuniformity of the poloidal component. In an ideal magnetic field topology with nested toroidal surfaces, the field line pitch is a surface property, expressed by the function $q(r)$.

However, our calculations demonstrate the existence of finite shear in perturbed topologies, by following 150 field lines with different initial radii (inside and outside chaotic regions), for N transits around the torus, with M initial poloidal angles for each starting radius.

The average q value, defined as

$$\langle q\rangle = M^{-1}\sum_{i=1}^{M} \overline{q_i},$$

with

$$\overline{q_i} = 2\pi N \theta_i^{-1}(N), \tag{6}$$

is computed as a function of the average radius $\langle r\rangle$,

$$\langle r\rangle = (2\pi NM)^{-1}\sum_{i=1}^{M} \int_0^{2N\pi} r(\phi,\theta_i)\,d\phi, \tag{7}$$

with ϕ the toroidal angle. Here $\theta_i(N)$ is the running poloidal angle, which started at θ_i, after N turns. The result is shown in Fig. 2 for the perturbing field with $b_\epsilon \approx 10^{-3}$ (shown in Fig. 1), and $N=M=100$.

In this plot, the positions of the large islands can be recognized by the gaps in the string of circles. The important conclusion of Fig. 2 is that in the chaotic regions the shear is not reduced. The perturbing fields do give rise to statistical variations in q, as can be judged from the values of $\sigma_{\langle q\rangle} \equiv \langle q\rangle^{-1}[\langle q^2\rangle - \langle q\rangle^2]^{1/2}$.

We have found these results to be independent of N in the range $1 \leqslant N \leqslant 200$ and independent of the spectrum (toroidal mode numbers up to 13 and poloidal mode numbers up to 14) and amplitude (ranging from 5×10^{-5} to 5×10^{-3}) of the perturbations. The limit $N=200$ is chosen on plasma physical grounds: A few hundred toroidal turns is an upper estimate of the mean free path of a thermal electron in the hot core of a tokamak. As the outcome is independent of N, the absence of shearless regions cannot be explained by a limited wandering of the field lines in the radial direction in chaotic regions. Indeed, we have found identical results for fields with stronger perturbations, where the field lines could cross large chaotic regions within 10 toroidal transits. Hence, we have demonstrated that shear does exist in the regions with chaotic magnetic field. In fact, the existence of finite shear in a chaotic layer is to be expected. The poloidal field component B_θ still exists after adding the perturbations and is much larger than the perturbation: $B_\theta/B_0 \approx 10^{-1}$ vs $b_\epsilon < 10^{-3}$. The answer to the question how B_θ can change in a region which is filled by a single field line, is that the field line does not visit every point in this region with the same frequency.

We now have to consider the effect of shear on transport: How does the presence of shear influence the divergence of the field lines? In the following we assume the profile $q(r)$ to monotonically increase with r, and consider the ϕ evolution of the cross section of a bunch of correlated field lines, which is initially circular with a radius s. Compared to the radial position r_c of the center of the circle, s is small.

We follow a set of field lines that, at $\phi=0$, lie on the circle. In an unperturbed field, we observe that at $\phi \neq 0$ the circle is stretched in poloidal direction. The reason is the

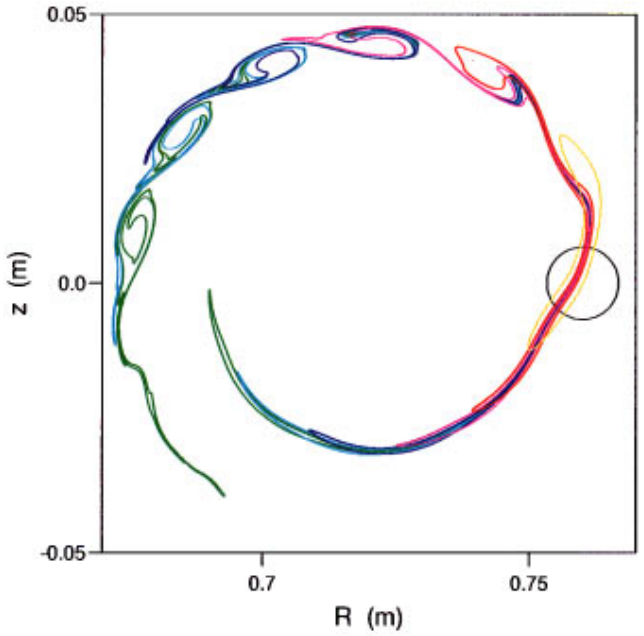

FIG. 3. Deformation of the cross section of a bunch of field lines in a chaotic region of the field shown in Fig. 1. Yellow, red, magenta, dark blue, light blue, and green correspond to one to six toroidal transits. The branch extending clockwise is close to the $q=1$ magnetic island, and shows the well-known stickiness of the island (almost no chaotic deformation).

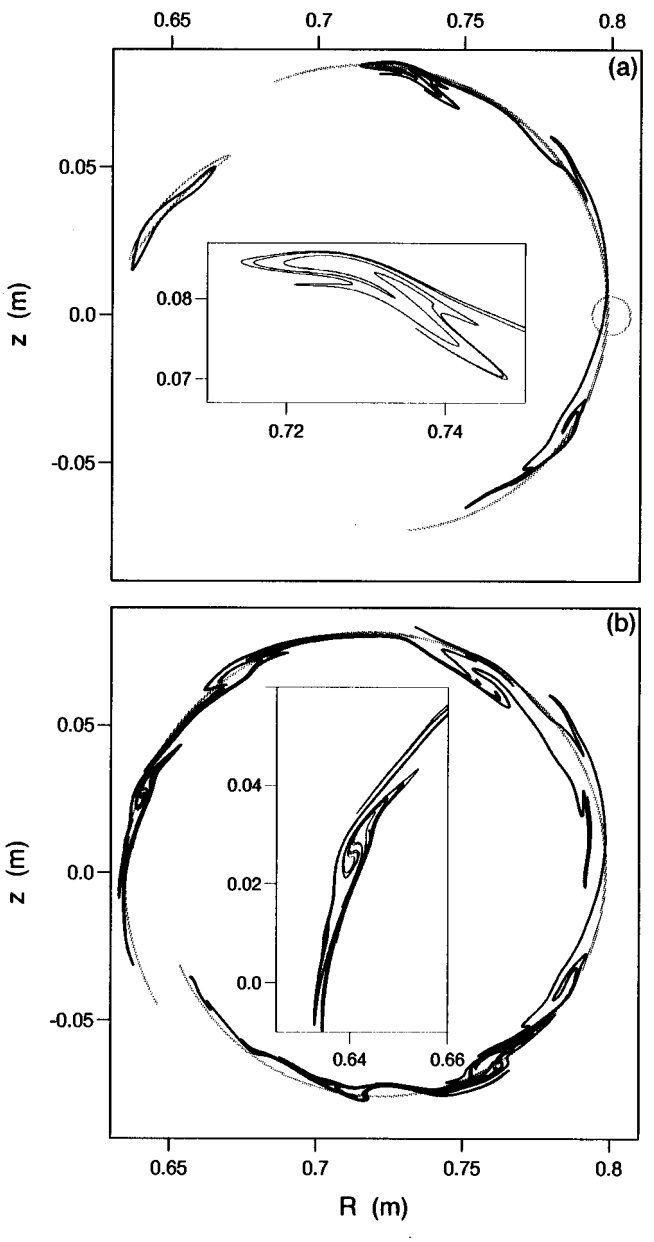

FIG. 4. Comparison of the deformation of a bunch of field lines in the perturbed magnetic field of Fig. 1 and an unperturbed field. Conditions as in Fig. 3, but with the center of bunch at a larger radius. Gray curves: the effect of shear alone; in black: the combined effect of shear and chaotic motion for (a) one and five and (b) ten toroidal transits. The gray circle in panel (a) is the initial bunch of field lines.

difference in q values of the surfaces on which the field lines lie, and not the hyperbolicity of the system. With the assumed $q(r)$ profile, the field line started at r_c+s will ''move'' slower (and the field line started at r_c-s will move faster) in the poloidal direction than the central field line. Due to the conservation of the magnetic flux through the deformed circle, the stretching in the poloidal direction is accompanied by a reduction of the width in the radial direction.

Obviously, the stretching does not give rise to an exponential divergence of field lines. Hence, in a chaotic magnetic field with a realistic shear, the divergence of field lines has a nonexponential contribution (due to the shear) and an exponential contribution (due to the chaotic motion). The latter appears when a perturbing field is added. We compared the growth rates of the arm lengths in cases with and without perturbing field. For a toroidal length scale of one to two transits, we found an increase of only 5%[16] for $b_\epsilon \sim 10^{-3}$. For more transits the chaotic behavior distorts the appearance of the circle in the radial direction, so that a comparison of growth rates is not feasible anymore. Exponential divergence will win in the long run, but also here the effect of shear still plays an important role, as we will demonstrate.

In Figs. 3 and 4 two examples are shown to illustrate the combined effect of an ideal magnetic field with an additional small perturbation.

We started 2×10^5 points on a small circle, for various field perturbations, produced with current filaments. The radius of the circle was chosen to be the average distance between the perturbing filaments. It is clear that shear plays a major role in the deformation of the circle; deformation is obviously biased toward the poloidal direction, in contrast to the assumption that deformation is as strong in the radial as in the poloidal direction, which is made in the cited literature.

Qualitatively the plots in Figs. 3 and 4 can be understood with arguments similar to those we gave earlier for the deformation of the circle in an ideal sheared magnetic field. Starting with a circle with radius $s \ll r_c$, the field lines with $r<r_c$ ''move'' faster in the poloidal direction and the field lines with $r>r_c$ lag behind.

Initially the chaotic movement due to the field perturbation is of secondary importance: stretching is the dominant effect. However, following the field lines over a longer in-

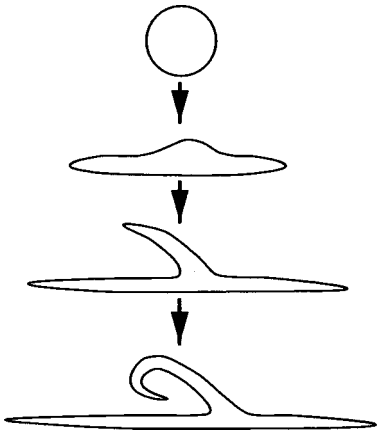

FIG. 5. Schematic explanation for the patterns in Figs. 3 and 4.

terval, the elongated cross section becomes distorted due to the chaotic movements in the radial direction. More arms will result from these distortions, and each individual arm will be subject to the effect of shear. This process is schematically illustrated in Fig. 5. A comparison with rolling water waves comes to mind.

An important observation is that the stretching is now a strongly inhomogeneous process; some parts of the bunch of field lines remain compact, while other parts undergo very strong stretching. This comes about because the majority of the field lines is trapped in ''rolling wave'' patterns, that become more and more compact and complex as a result of the repeated folding of the branches [e.g., Fig. 4(b)]. Consequently, the arms connecting these compact structures become infinitely thin. Because of the compact regions connected with infinitely stretched regions, it is unclear whether or not exponential divergence is a correct picture for the decorrelation processes. Since the divergence due to shear alone is in a first approximation linear in ϕ, the combined effect of the two processes is at least linear. However, if it is exponential, characteristic lengths for a sheared field should play an important role in the exponential decay length.

Krommes *et al.*[10] investigated just this in the framework of quasilinear theory for a magnetic field with a relatively weak background shear. The tokamak, however, is in the region with relatively strong shear.

Although we have restricted ourselves to tokamaks in this discussion, the conclusions are in fact generic for Hamiltonian systems with shear.

IV. RADIAL TRANSPORT IN CHAOTIC LAYERS

Bearing in mind that we should take shear into account in the chaotic regions, we will now have a closer look at the behavior of the field lines in these regions.

In the literature, a ''Brownian'' motion of the field lines is usually assumed, described by an Ornstein–Uhlenbeck process. Inherent in such a process is an infinite spectrum of perturbing modes, frequently approximated by a large number of poloidal mode numbers m (as, e.g., in Ref. 19), or toroidal mode numbers n (e.g., in Ref. 20), or both. With such a spectrum of modes, a fundamental problem arises. In a tokamak, the perturbing fields are generated by the current distribution inside the plasma. The current perturbations must be field aligned or nearly so. Hence, the allowed modes for current perturbations have $m/n \sim q$, where q is the local safety factor. Since high-m current perturbations have a short range, at any place in the plasma only low mode numbers and mode numbers centered around $m/n = q$ are felt. Thus, a wide, global spectrum of perturbing modes, and so the assumption of Brownian field line motion, is unphysical.

Figures 6(b) and 6(e) show contours of the rms radial displacement (σ) of a field line as a function of its starting radius r_0 and the toroidal angle ϕ, averaged over 500 field lines with the same r_0. This representation highlights the layered structure of the magnetic topology: layers in which field lines make large radial excursions alternate with layers with ''good'' surfaces. The same quantity is plotted for five starting positions of field lines in Figs. 6(c) and 6(f) to show that three types of behavior can be discerned: field lines that stay close to r_0 (nonstochastic or very thin stochastic regions); field lines that exhibit oscillatory behavior (caught within or very close to magnetic islands); and field lines taking large radial steps for a few toroidal transits and traveling much more slowly thereafter (chaotic regions). Importantly, none of these three types of excursions can be characterized as a Brownian motion.

Although D_M can only be properly defined in the long time limit of the Ornstein–Uhlenbeck process, we can ask whether concentrating the discussion on the chaotic regions could result in a useful D_M. Selecting field lines in these regions and averaging their trajectories, results in an average displacement as a function of toroidal angle, $\langle \sigma(\phi) \rangle$, as depicted in Fig. 7. Curves are shown for different levels of b_ϵ, demonstrating that the shape of $\langle \sigma(\phi) \rangle$ is almost independent of b_ϵ. Clearly, this displacement is not a Gaussian random walk, which would have $\langle \sigma \rangle \propto \phi^{1/2}$, so D_M cannot be defined. A good fit to the curves is given by

$$\langle \sigma \rangle \propto \begin{cases} \ln(1+0.2\phi), & \pi < \phi < 20\pi \\ \phi^{1/4}, & \phi > 20\pi \end{cases} . \tag{8}$$

By inspection of the field line distribution as a function of the number of toroidal transits, boundary effects were excluded as a cause of the roll-over.

The same procedure has been carried out with different sets of current filaments, and also with global perturbations (mode numbers up to $m = 12$) instead of current filaments, and with our sets of initial conditions for the field lines, the qualitative behavior of $\langle \sigma(\phi) \rangle$ was always the same.

V. TEST PARTICLE TRANSPORT

Making the step from field line behavior to test particle transport, we follow the classical treatment,[9] using two modifications. First, the probabilistic description of a non-Gaussian process is too complex to define a value for D_M, forcing us to resort to the numerical results of our simulations for the average field line behavior in a chaotic field i.e., the $\sigma_{\ln}$ and $\sigma_{1/4}$ curves shown in Fig. 7. Second, because the field line trajectory is superdiffusive on the short track, but subdiffusive in the long run, we need to distinguish between

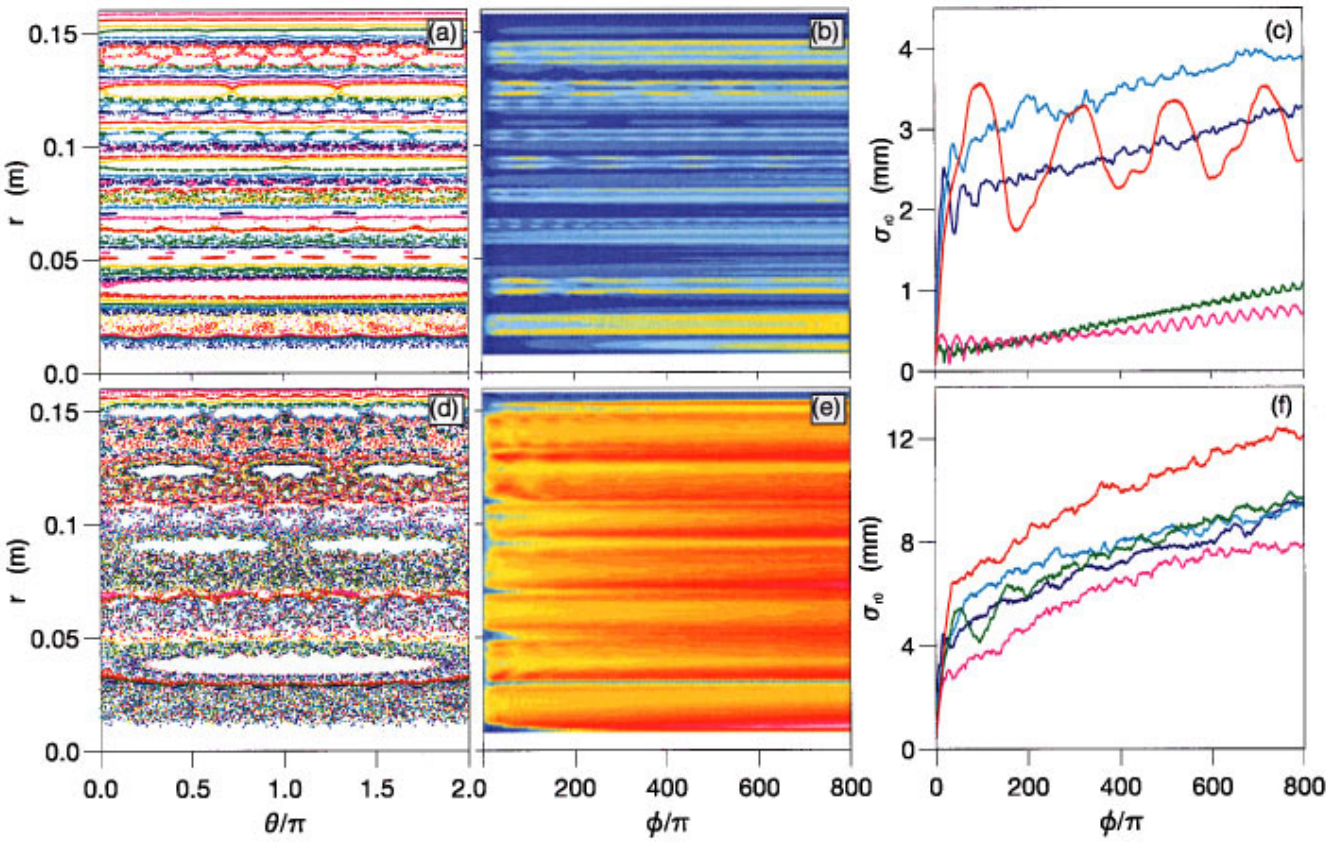

FIG. 6. For a slightly perturbed magnetic field with the perturbing part induced by 19 current filaments, with $b_\epsilon \propto 2\times10^{-4}$ and $b_\epsilon \propto 10^{-3}$ for the top panels and the bottom panels, respectively. (a) and (d) Poincaré plots. (b) and (e) The average displacement $\sigma_{r0}(\phi)$ as a function of the initial radial position r_0. (c) and (f) Projections of the contour plots (b) and (e), respectively, for five different starting positions r_0 each. The colors of the contour plots run from blue via yellow to red, where dark blue signifies the smallest values of σ_{r0} (up to 0.5 mm) and pink the largest ($\sigma_{r0}>14$ mm). The Poincaré plots were produced from 60 orbits with 600 transitions each.

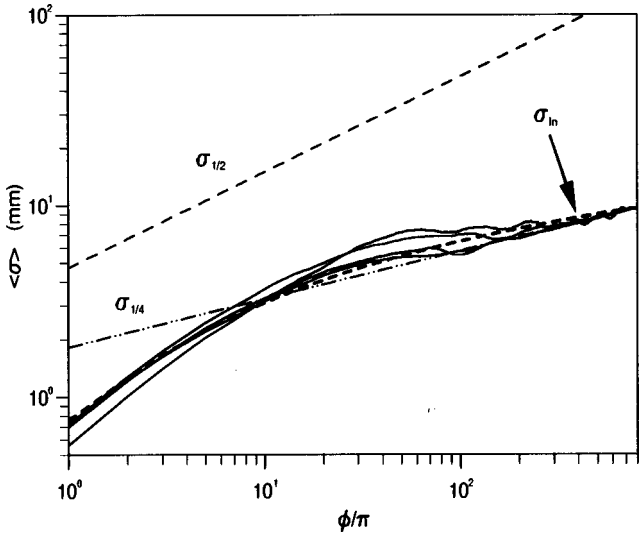

FIG. 7. The average displacement $\langle\sigma\rangle$ in chaotic regions, as a function of the toroidal angle ϕ, as observed in numerical simulations. The solid lines represent the data for values of b_ϵ between 10^{-5} and 10^{-3}, scaled to the $b_\epsilon=10^{-3}$ data. For $\pi<\phi<20\pi$ a good fit is given by $\sigma_{\ln}\propto\ln(1+0.2\phi)$ and for large ϕ by $\sigma_{1/4}\propto\phi^{1/4}$. The dashed line labeled $\sigma_{1/2}$ is the quasilinear diffusion prediction for $b_\epsilon=10^{-3}$, using a numerically determined value for $L_{c\|}$.

discrete collisions (a discrete radial step of size ρ_e after a time τ_c) and continuous small angle scattering. The latter process gives the dominant contribution to the effective collision frequency in a hot plasma. For the actual decorrelation of the test particles from their field lines, various mechanisms are proposed in the literature, which combined with our findings so far, lead to different scalings of χ with $v_\|$. Several mechanisms are discussed below, and the resulting scalings can be found in Table I. The diffusivity is calculated from $\chi\equiv\langle\sigma^2(z(t_d))\rangle/(2t_d)$, with t_d the decorrelation time, z the distance traveled along the magnetic field line, and σ given by 8 for nondiffusive field lines, and

$$\langle\sigma^2(z)\rangle=\begin{cases}2D_M z, & z>L_0\\ b_0^2 z^2 & z<L_0\end{cases} \tag{9}$$

for diffusive field lines, with L_0 the correlation length along the magnetic field line. Note that discrete collisions and continuous scattering do only lead to different scalings of χ with $v_\|$ for the case of sheared non-Gaussian field lines.

In the case of small angle scattering, the distance $\delta(t)$ between the test particle and the field line it started on, increases in time as $t^{1/2}$. Simultaneously, due to the chaotic motion of the field lines, the step $\delta(\phi)$ needed to move to an

TABLE I. The effect of using non-Gaussian behavior of magnetic field lines combined with sheared decorrelation, as compared to the classical picture of Gaussian field lines being exponentially decorrelated for three different decorrelation mechanisms. The velocity parallel (perpendicular) to the magnetic field **B** is denoted $v_\parallel$ ($v_\perp$) and the **E×B** drift velocity is written v_E. The sheared non-Gaussian case corresponds to typical tokamak conditions.

	Exponential		Sheared	
	Gaussian	non-Gaussian	Gaussian	non-Gaussian
Discrete collisions	$v_\parallel$	$v_\parallel$	$v_\parallel$	$v_\parallel v_\perp^{1/2}$
Continuous scattering	$v_\parallel$	$v_\parallel$	$v_\parallel$	$v_\parallel^{1/3} v_\perp^{1/3}$
E×B drifts	$v_\parallel$	$v_\parallel$	$v_\parallel$	$v_\parallel^{2/3} v_E^{1/3}$

uncorrelated field line, decreases. This decrease is exponential in a shearless, fully chaotic field. However, as is demonstrated in Sec. III, with perturbation levels in a realistic range ($b_\epsilon \lesssim 10^{-3}$), shear remains important in chaotic layers and is indeed the dominant cause for the divergence of field lines.

A test particle now makes a random radial step when at $t=t_d$ the gyroradius $\rho_e=\delta(\phi)$. Through ρ_e, the perpendicular velocity, $v_\perp$, enters into the expression for χ.

Table I shows that using numerically determined field line trajectories instead of a Brownian motion of field lines and the quasilinear estimate of the associated D_M, results in a weaker scaling with $v_\parallel$ (except for discrete collisions).

For realistic values of $b_\epsilon \lesssim 10^{-3}$, the value of χ due to collisional decorrelation in the chaotic magnetic field is lower than the experimental value $\chi \sim 1\ \mathrm{m^2\,s^{-1}}$, as can be seen in Fig. 8. Therefore, it cannot explain the measured anomalous electron transport. Additional decorrelation mechanisms are called for if magnetic turbulence is to cause the the electron transport anomaly.

One obvious decorrelation mechanism is a time dependence of the magnetic field perturbations. While in the above a static field was assumed, in a tokamak plasma the field

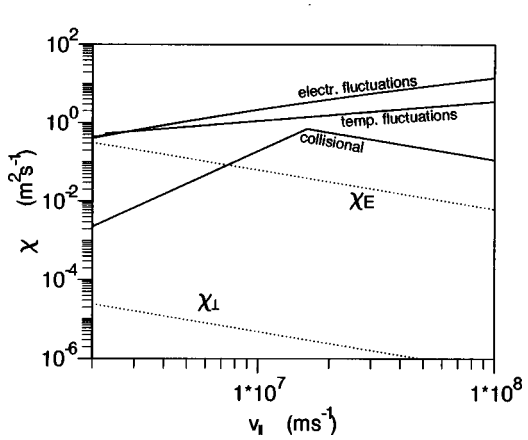

FIG. 8. The diffusion coefficient χ is plotted as a function of the velocity $v_\parallel$ parallel to the magnetic field for a magnetic perturbation level $b_\epsilon \approx 10^{-3}$. Three different decorrelation mechanisms are plotted here: collisions, electrostatic fluctuations (with **E×B** drift velocity v_E), and temporal fluctuations (with frequency f). $\chi_\perp$ and χ_E have been plotted as well for comparison. For the computations $n_e=4\times10^{19}\,\mathrm{m^{-3}}$, $v_E=500\,\mathrm{ms^{-1}}$, and $f=100\,\mathrm{kHz}$ are used. Changing v_E or f within a factor of 10, changes the curves for electrostatic and temporal fluctuations by a factor of 1.5 and 3, respectively. A change of n_e over a factor 3 does not bring significant changes.

perturbation must be regarded as magnetic turbulence. Experimental spectra of magnetic fluctuations measured in Tore Supra typically extend to frequencies f of several hundreds of kilohertz. Crudely assuming that particles are decorrelated from the field every 10 μs, results in a significant increase of χ, with a factor $\sim$2, bringing it in the range of the experimental values for $b_\epsilon = 10^{-3}$ (see Fig. 8).

As a new mechanism enhancing χ, synergistic effects of electrostatic and magnetic turbulence are proposed. In this case, the fluctuating **E×B** drifts cause the test particle to decorrelate from the field line. Now the electrostatic fluctuations cause the decorrelation, while the step size is determined by the excursions of the magnetic field lines. To make a rough estimate of this the effect, a constant drift velocity $v_E = 500\,\mathrm{m/s}$, based on experimental work in the Texas Experimental Tokamak TEXT,[21] can be used. This results in decorrelation times of 2–20 toroidal turns, enlarging χ with a factor $\sim$5, bringing it in the range of experimental values ($\chi \sim 1\ \mathrm{m^2\,s^{-1}}$) (see Fig. 8). The resulting scaling of χ is put in Table I for comparison.

VI. CONCLUSIONS AND DISCUSSION

In summary, we have found that the divergence of field lines in a chaotic field in a tokamak differs essentially from the picture by Rechester and Rosenbluth[9] and subsequent papers by others. A strong poloidal background field results in a divergence of field lines that is dominated by simple stretching. Only after many toroidal transits does the perturbing part of the field show its influence. The effects of a sheared field in the poloidal direction with an additional small perturbing field on the resulting picture could be understood qualitatively. From our computations and arguments it does not seem to be justified to neglect the effect of shear when considering chaotic magnetic fields.

Also, we find that even at perturbation amplitudes as high as $b_\epsilon = 10^{-3}$, the tokamak field does not become fully chaotic, but retains a structure of nested shells. In the chaotic regions, the excursions of field lines differ essentially from Brownian motions. The behavior goes from superdiffusive to subdiffusive as the toroidal angle grows. Test particle transport is significantly smaller than predicted by Eq. (2), unless additional mechanisms are invoked to decorrelate the test particles from the field lines, such as temporal fluctuations of the magnetic field or electrostatic fluctuations. Interestingly, the scaling of test particle diffusivity with $v_\parallel$ is weaker than linear, which is significant in the view of the observation that runaway electrons often show superior confinement.[22]

Based on our findings, transport theories in chaotic magnetic fields should deal with three adjustments: (i) the divergence of field lines is not exponential, (ii) the folding and stretching process is very complex, resulting in inhomogeneous divergence, and (iii) decorrelation of the particle inside a compact structure may not lead to actual decorrelation, as field lines that were correlated at the start are still close by. In contrast, other parts of a bunch of field lines undergo very strong stretching, which might lead to fast decorrelation and result in a strong contribution to transport.

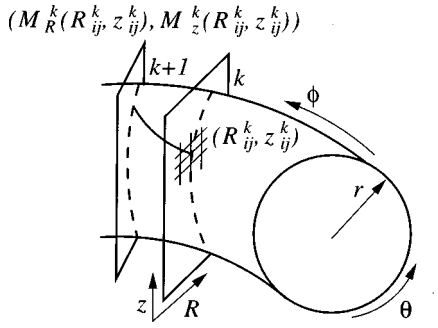

FIG. 9. Graphical illustration of the mapping technique used for computing the magnetic topology. The field lines are mapped from a grid point (i,j) on section k to section $k+1$ by integration of the field line equations. Also shown are the directions of the unit vectors.

To finish the discussion, we stress that although in this work we have restricted ourselves to regions of stochastic field line trajectories, a complete description of transport in a tokamak should incorporate both regions of chaotic field and regions of quiescent magnetic field. Until recently, it has been beyond experimental capabilities to distinguish between these regions. Now, in Ref. 23 it has been reported that the picture of a tokamak plasma consisting of alternating layers of good and bad confinement can in fact be reproduced experimentally, putting experiment and theory into better agreement.

ACKNOWLEDGMENTS

This work was carried out under the Euratom–FOM agreement, with financial support from Nederlandse Organisatie voor Wetenschappelyk Onderzoek (NWO) and Euratom.

APPENDIX

The numerical techniques for calculating the perturbed magnetic tokamak field are based on the mapping techniques first presented in Ref. 15. This procedure was originally developed to solve Hamiltonian systems and can be sketched as follows.

Assume that the magnetic field **B** is known in toroidal coordinates (R,ϕ,z) (see Fig. 9 for the coordinate definitions). The magnetic field may have the axially symmetric form of Eq. (3), but any type of perturbation may be added. The three-dimensional toroidal space is covered by a grid of N_ϕ planes, equally spaced in the ϕ coordinate with angular separation $\Delta\phi = 2\pi/N_\phi$ and each plane is covered with a rectangular grid in the R and z coordinates. The minimum size of the grid is chosen to cover the entire plasma volume. Using indices ijk, the coordinates of the grid points in the coordinates (R,ϕ,z) are labeled R_{ij}^k and z_{ij}^k on cross section k at the toroidal angle $\phi = (k-1)\Delta\phi$. The magnetic field **B** is evaluated on each grid point.

The next step is the construction of the mapping functions $M_R^k(R,z)$ and $M_z^k(R,Z)$. These functions compute the position $(R^{k+1},z^{k+1}) = (M_R^k(R^k,z^k), M_z^k(R^k,z^k))$ of the field line intersection with the $(k+1)$th plane, knowing that it has crossed the kth plane at (R^k,z^k). This set of functions is created by numerically integrating the field line equations

$$\frac{dR}{d\phi} = R\frac{B_R}{B_\phi}, \quad \frac{dz}{d\phi} = R\frac{B_z}{B_\phi}, \tag{A1}$$

from a grid point (R_{ij}^k, z_{ij}^k) on the kth plane to the point on the $(k+1)$th plane $(M_R^k(R_{ij}^k, z_{ij}^k), M_z^k(R_{ij}^k, z_{ij}^k))$ (see Fig. 9). Spline interpolation schemes between grid points are used to construct the functions over the whole plane. In this way the function $M_R^k(R,z)$ gives the R coordinate at plane $(k+1)$ for a field line started at (R,z) on plane k, and similarly for $M_z^k(R,z)$ and the z coordinate. The functions M_R^k and M_z^k with $k = N_\phi$ complete the circle in the toroidal direction.

For the integration scheme, we use the generic Hamiltonian property of conservation of area to ensure numerical accuracy. The magnetic field components are interpolated with a spline interpolation scheme over the poloidal planes and with a fourth-order Lagrange polynomial interpolation between planes.

Using the mapping functions, the motion of a field line is described by the series of points (R^l,z^l) for $l = 1,\ldots,N_{\text{tor}}N_\phi$ of crossings with the poloidal planes, starting from the initial point (R^1,z^1); N_{tor} gives the total number of revolutions around the torus.

[1] J. Wesson, *Tokamaks*, 2nd ed. (Clarendon, Oxford, 1997).
[2] P. C. Liewer, Nucl. Fusion **25**, 543 (1985).
[3] C. M. Greenfield, D. P. Schissel, B. W. Stallard, E. A. Lazarus, G. A. Navratil, K. H. Burrell, T. A. Casper, J. C. DeBoo, E. J. Doyle, C. B. Fonck, R. J. Forrest, P. Gohil, R. J. Groeber, M. Jakubowski, L. L. Lao, M. Muraki, C. C. Petty, C. L. Rettig, T. L. Rhodes, B. W. Rice, H. E. St. John, G. M. Staebler, E. J. Strait, T. S. Taylor, A. D. Turnbull, K. L. Tritz, R. E. Waltz, and the DIII-D Team, Phys. Plasmas **4**, 1596 (1997).
[4] R. J. Bickerton, Plasma Phys. Controlled Fusion **39**, 339 (1997).
[5] X. L. Zou, L. Colas, M. Paume, J. M. Chareau, L. Laurent, P. Devynck, and D. Gresillon, Phys. Rev. Lett. **75**, 1090 (1995).
[6] N. J. Lopes Cardozo, F. C. Schüller, C. J. Barth, C. C. Chu, F. J. Pijper, J. Lok, and A. A. M. Oomens, Phys. Rev. Lett. **73**, 256 (1994).
[7] M. N. Rosenbluth, R. Z. Sagdeev, J. B. Taylor, and G. M. Zaslavsky, Nucl. Fusion **6**, 297 (1966).
[8] V. I. Arnold, *Geometrical Methods in the Theory of Ordinary Differential Equations* (Springer, New York, 1983).
[9] A. B. Rechester and M. N. Rosenbluth, Phys. Rev. Lett. **40**, 38 (1978).
[10] J. A. Krommes, C. Oberman, and R. G. Kleva, J. Plasma Phys. **30**, 11 (1983).
[11] M. B. Isichenko, Plasma Phys. Controlled Fusion **33**, 795 (1991).
[12] H. Wang, M. Vlad, E. Vanden Eijnden, F. Spineanu, J. H. Misguich, and R. Balescu, Phys. Rev. E **51**, 4844 (1995).
[13] J. H. Misguich, M. Vlad, F. Spineanu, and R. Balescu, in *Transport, Chaos and Plasma Physics 2, Marseille, 1995*, edited by S. Benkadda, F. Doveil, and Y. Elskens (World Scientific, Singapore, 1996), p. 209.
[14] E. Vanden Eijnden and R. Balescu, Phys. Plasmas **4**, 270 (1997).
[15] A. Montvai and D. F. Düchs, in *Physics Computing '92, Prague, 1992*, edited by R. A. de Groot and J. Nadrchal (World Scientific, Singapore, 1993), p. 417.
[16] M. de Rover, Ph.D. thesis, Eindhoven University of Technology, 1996.
[17] R. Balescu, *Transport Processes in Plasmas* (North-Holland, Amsterdam, 1988), Vol. 2.
[18] F. C. Schüller, D. C. Schram, J. Konings, A. C. A. P. van Lammeren, J. C. M. Timmermans, M. Verreck, and the RTP team, in *Controlled Fusion and Plasma Physics, Berlin, 1991*, edited by P. Bachmann and D. C. Robinson (European Physical Society, Petit-Lancy, 1991), Vol. 4, p. 185.
[19] R. B. White and Y. Wu, Plasma Phys. Controlled Fusion **35**, 595 (1993).
[20] J. R. Cary, D. F. Escande, and A. D. Verga, Phys. Rev. Lett. **65**, 3132 (1990).
[21] A. J. Wootton, in *Transport, Chaos and Plasma Physics, Marseille, 1993*,

edited by S. Benkadda, F. Doveil, and Y. Elskens (World Scientific, Singapore, 1994).
[22]J. Jaspers, N. J. Lopes Cardozo, K. H. Finken, B. C. Schokker, G. Mank, G. Fuchs, and F. C. Schüller, Phys. Rev. Lett. **72**, 4093 (1994).
[23]N. J. Lopes Cardozo, G. M. D. Hogewij, M. R. de Baar, M. N. A. Beurskens, F. De Luca, A. J. H. Donné, P. Galli, J. F. M. van Gelder, G. Gorini, B. de Groot, A. Jaccia, F. A. Karelse, J. de Kloe, O. G. Kruijt, J. Lok, P. Mantica, H. J. van der Meiden, A. A. M. Oomens, T. Oyevaar, F. J. Pijper, R. W. Polman, F. Salzedas, F. C. Schüller, and E. Westerhof, Plasma Phys. Controlled Fusion **39**, B303 (1997).